Research Square

Preprints are preliminary reports that have not undergone peer review.
They should not be considered conclusive, used to inform clinical practice,
or referenced by the media as validated information.

Robotic Arm-Assisted Droplet-Based Additive Manufacturing via Acoustic Levitation: Process Implementation and Experimental Optimization

Ye Li

yli@bumail.bradley.edu

Bradley University https://orcid.org/0000-0003-1292-9346

Umamaheswara Ra Datla

Noah Negron

Research Article

Keywords: Tankless Additive Manufacturing, Droplet, Robotic Arm, Acoustic Levitation, Contactless Manufacturing

Posted Date: June 25th, 2026

DOI: https://doi.org/10.21203/rs.3.rs-10031598/v1

License: This work is licensed under a Creative Commons Attribution 4.0 International License.
Read Full License

Robotic Arm-Assisted Droplet-Based Additive Manufacturing via Acoustic Levitation: Process Implementation and Experimental Optimization

Ye Li*, Umamaheswara Ra Datla, and Noah Negron

Department of Industrial and Manufacturing Engineering and Technology
Bradley University, Peoria, IL USA
* Corresponding author, Tel. 309-677-2934, Fax 309- 677-2853, E-mail: yli@bradley.edu

Abstract
This paper presents the concept, implementation and process optimization of a robotic arm-assisted additive manufacturing system using acoustic levitation for droplet-based deposition of photocurable resin. By integrating acoustic levitation and robotic manipulation, the tank-free material deposition approach has the potential to overcome the limitations inherent in conventional 3D printing - such as fixed build directions, planar layers and the reliance on resin tanks. The focus of this study is on experimental characterization and process optimization. Necessary aspects of implementing the additive manufacturing system were investigated, including the ultraviolet (UV) light profile characterization, resin curing characterization and contact angle measurement. A Taguchi experiment- based process optimization further revealed the optimal combination of process parameters for surface quality on continuously deposited droplets. Implementation of the system was demonstrated using a commercial photocurable resin. This work paves the way for the development of a multi-material contactless and tankless additive manufacturing platform that supports multi-directional deposition.

Keywords: Tankless Additive Manufacturing; Droplet; Robotic Arm; Acoustic Levitation; Contactless Manufacturing;

1. Introduction

Additive manufacturing has transformed production by imparting both greater design flexibility and broader material accommodation. However, traditional additive manufacturing systems remain constrained by several fundamental limitations. Most 3D printing processes rely on sequential deposition of 2.5-D planar layers along a fixed build direction. In addition, support structures are often required to uphold overhanging features against gravity during printing which must be removed afterwards. Further, the reliance on build plates, resin tanks and support structures as well as their associated removal and cleaning processes potentially introduce contamination and cause mechanical damage during post-processing. To address these limitations, this paper presents a robotic arm-assisted droplet additive manufacturing system based on acoustic levitation and localized photopolymerization.

A major limitation of conventional additive manufacturing is the requirement to select a single build direction in process planning. Researchers have investigated criteria for build direction selection such as surface finish, construction height, support structure, manufacturing efficiency, structure strength, etc **[Li and Zhang 2013]**. The layered effect inherent to additive

manufacturing often leads to volumetric deviation between the printed object and the corresponding design model **[Rattanawong et.al. 2001, Masood and Rattanawong 2002, and Kumar and Choudhury 2005]**. Moreover, the bonding strength between layers is often a structural weak point in 3D printed workpieces and printing machines have dimensional constrains for build volume. To improve print performance, numerous optimization strategies have been developed. Shen et.al. **[Shen et.al. 2020]** included build efficiency, surface finish and mechanical properties into a particle swarm framework. Selvam et. al. **[Selvam et. al. 2022]** employed particle swarm optimization and response surface methodology to optimize print time and surface quality in fused filament fabrication. Li and Zhang **[Li and Zhang 2013]** implemented a multi- criteria genetic algorithm to optimize theoretical volume deviation and part height while Günaydın et. al. **[Günaydın et. al. 2022]** and Matos et. al. **[Matos et. al. 2021]** extended their optimization to support structure generation and other competing objectives. Although current research on build direction optimization addressed multi- objective scenarios, the solution set is restricted to a single direction due to the constraints imposed by 3D printing machine setup.

To overcome the constraint of a single build direction imposed by flat layers, curved layer additive manufacturing has been proposed. Curved layer fabrication has been mainly implemented on 5-axis printers **[Jee and Kim 2017, Duarte et.al. 2022, Hong et. al. 2023]** and robotic systems **[Xie et.al. 2020, Fry et.al. 2020, Fang et.al. 2024, İpekçi and Ekici 2024]**. By depositing materials conforming to the local geometric curvature, curved layers can reduce staircase effects, improve surface finish and more importantly enhance mechanical properties. Fry et.al. **[Fry et.al. 2020]** reported that tensile force resulting from curved layers improved over 50% compared to that from conventional flat layers. Fang et.al. **[Fang et.al. 2024]** further demonstrated that maximum enhancement in failure load and stiffness reached up to 544% and 140%, respectively through stress-aligned continuous-fiber printing. Despite these advantages, curved layer fabrication introduces increased complexity in slicing algorithms, toolpath generation and machine control.

In addition to process planning constraints, vat photopolymerization technologies such as stereolithography (SLA) and digital light processing (DLP) rely on resin tanks to contain liquid photocurable materials. Excess resin can remain on the printed surfaces or become trapped inside the geometric features, necessitating post-processing cleaning operations. Previous studies have shown that post-cleaning factors, including cleaning agents, cleaning duration and cleaning methods, significantly influence surface quality, hardness, degree of polymerization and mechanical properties such as flexural strength and fracture loads **[Long et. al. 2024, Katheng et. al. 2025, Mayer et. al. 2021, Lambart et.al. 2022, Jin et.al. 2022, Xu et.al. 2021].** In the meantime, post-cleaning is particularly important for medical and dental applications because uncured resin and photoinitiators contribute to cytotoxicity. Hwangbo et. al. **[Hwangbo et. al. 2021]** experimentally demonstrated that increasing post cleaning time significantly improves cell viability and reduces cytotoxicity. However, prolonged cleaning has been shown to reduce mechanical properties such as, microhardness **[Oh et.al. 2023]**, flexural strength **[Xu et.al. 2021, Oh et.al. 2023]** and flexural modulus **[Hwangbo et. al. 2021]**. Consequently, an inherent tradeoff exists between biocompatibility and mechanical performance. This challenge

is fundamentally associated with the requirement to maintain a bulk reservoir of liquid resin throughout the 3D printing operations.

Acoustic levitation has been investigated for material handling and assembly applications. Recent advances in acoustic research have demonstrated that acoustics can assist material sorting in metal additive manufacturing **[Ye et.al. 2026]** and contactless material manipulation **[Chen et.al. 2025, Foresti et.al. 2018]**. The ability to manipulate materials without direct contact offers a feasible pathway towards overcoming several limitations of conventional additive manufacturing. However, the integration of acoustic levitation into additive manufacturing remains limited, particularly for the controlled manipulation and photopolymerization of photocurable resin droplets using robotic systems. By suspending photocurable droplets in mid-air and combining acoustic levitation with robotic manipulation, material deposition can be decoupled from a fixed build direction. The approach has the potential to reduce dependence on support structures and eliminate the need for a resin containment tank during fabrication.

In this paper, we present the concept, implementation and experimental optimization of a robotic arm assisted droplet based additive manufacturing system utilizing acoustic levitation and localized photopolymerization. Unlike conventional layer-based additive manufacturing processes, the proposed approach has the potential to address the current limitations associated with fixed build directions, planar layers, support structures and reliance on resin tanks. Using a commercial photocurable resin as the example material, experimental characterization of ultraviolet (UV) curing behaviors, resin properties and droplet contact angle measurement were conducted to establish process foundation. Although the resin itself is commercially available, the proposed approach relies on curing of levitated droplets rather than conventional vat-based photopolymerization, and therefore characterization of the UV light field and resin curing behavior is required to establish process window of fabrication parameters. A designed experiment was subsequently performed to identify significant process parameters and determine their optimal levels. The work presented herein represents an initial step toward a more flexible, contactless and tank-free additive manufacturing framework. The remainder of the paper is organized as follows. **Section 2** provides an overview of the process. **Section 3** describes the UV light characterization. **Section 4** covers the resin characterization. **Section 5** presents the contact angle measurement. **Section 6** outlines the process optimization, followed by a discussion in **Section 7**. **Section 8** concludes the paper.

2. Process Overview

With the purpose of implementing a tankless and contactless manufacturing, the proposed additive manufacturing strategy integrates four functionalities that traditional 3D printing machines cannot supply. First, the process must involve the suspension of a droplet of photocurable resin in the middle of air. This step allows for the fixation of the building block of the additive manufacturing while under the influence of gravity. Second, a moving print bed must be created such that it can be moved adjacent to the droplet in suspension for deposition. This functionality demands a level of dexterity that traditional 3-axis gantry structure used in most 3D printing machines can not provide. Further the mechanism used to maneuver the

moving printing bed should be programmable. Third, the deposition of resin droplets needs to be cured in order to form an attachment to the moving printing bed. Therefore, a source of UV light will be used to trigger the activation and maintain the continuation of transiting liquid resin droplets into fully cured building materials. Unlike acoustic transport systems where the droplet is translated through manipulation of the acoustic field, this approach maintains the droplet at a fixed levitation location while the robotic arm repositions the growing structure relative to the levitated droplet.

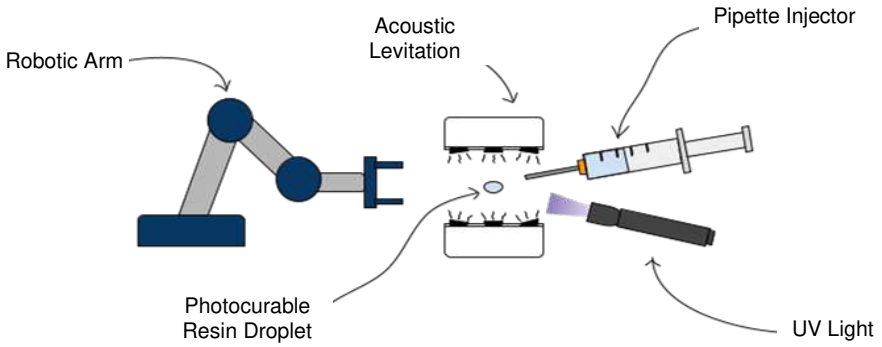
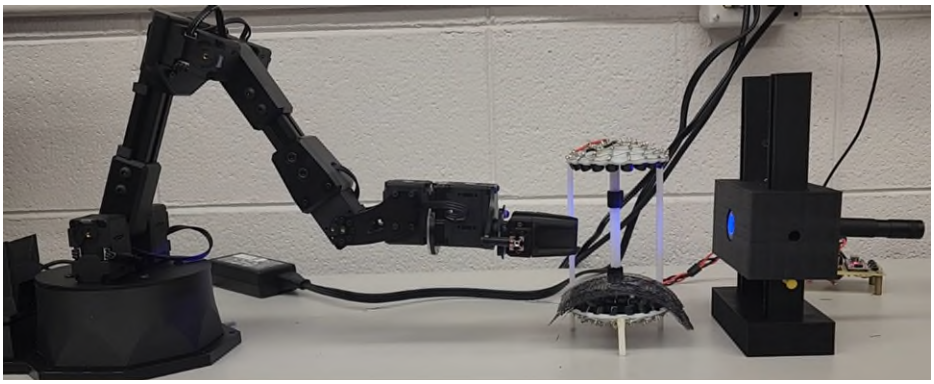
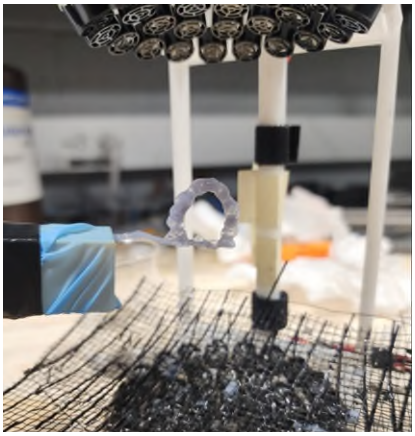


Figure 1. Schematic illustration of the proposed robotic arm-assisted acoustic levitation additive manufacturing process. Photocurable resin droplets are acoustically levitated and cured by UV irradiation. A robotic arm positions the growing structure to contact and incorporate the levitated droplet, enabling layer-free three-dimensional fabrication.

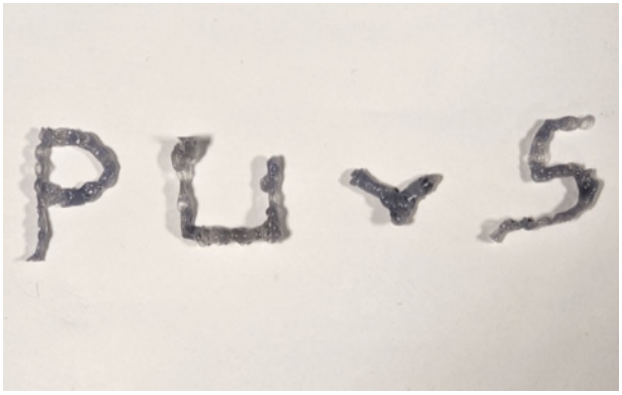
To fulfill the above- mentioned functionalities, the experiment setup is illustrated in **Figure 1,** consisting of four major units: an acoustic levitator, a 5 degree-of freedom robotic arm, a pipette injector and a UV light source. The process begins with a droplet of photocurable resin injected by the pipette injector to the working zone of the acoustic levitator. The acoustic levitator (TinyLev levitator from Makerfabs, China) is responsible for suspending the photocurable resin droplet during the Additive Manufacturing process. The acoustic levitator contains an array of acoustic transducers that together generate sound waves to counteract the gravity and keep the droplet in mid-air. This device specifically supports the concept of *Contactless Manufacturing.* With the droplet suspended in mid-air, a 5 degree-of freedom robotic arm (Model: Pincher X-150, from Trossen Robotics, USA) approaches the suspended droplet with its end effector connected to a moving print bed. The robotic arm positions the growing structure to contact and incorporate the levitated droplet, enabling layer-free three-dimensional fabrication. The process is repeated in this way with droplets incrementally deposited to the structure held by the robot arm end effector. As the robotic arm is able to maneuver with a wide range of motion that 3-axis gantry structure can not supply, this printing process allows for the creation of complex geometries with photocurable resins. **Figure 2** demonstrates the experimental implementation of the proposed manufacturing process, including the hardware setup, in-process fabrication, and representative fabricated samples.



2(a)



2(b)



2(c)

Figure 2. Experimental implementation of the robotic arm-assisted acoustic levitation additive manufacturing system: (a) experimental setup showing the acoustic levitator, robotic arm, UV curing system, and supporting hardware; (b) fabrication process during deposition and curing of levitated photocurable resin droplets; and (c) representative workpieces fabricated using the proposed process.

3. UV light profile characterization

Characterization of UV light profile must be carried out before the optimization of the additive manufacturing process. As the source of energy used to cure the levitated resin droplet, UV light distance, intensity and distribution profile directly influence the curing process kinetics. A UV light (Model: FL16R-UV 395nm ultraviolet from Cosmoing China) was employed in this work to cure the resin droplets. The UV light profile was measured on an experimental setup consisting of a lathe with its chuck holding the UV light and a chartboard attached to the tool post of the lathe (**Figure 3**). The experimental setup allowed for the chartboard to be set at different axial distances from the UV light. For this experiment 5, 10, and 15 cm were the tested distances from the chartboard. In the meanwhile, concentric circles were drawn on the chartboard with the center aligned with the lathe spindle axis. As the ultraviolet light was turned on, the emitted light was projected onto the chartboard. This experimental setup allows for the data collection to

create a profile demonstrating the varying light intensity on the chartboard at different radial distances. A light meter (Model: UV512C from General Tools, USA) was employed in the experiment to measure light intensity along the four different axes on the chartboard: a horizontal axis, a vertical axis, and two 45-degree cross axes. The collected data was then analyzed through the use of a Gaussian model, which was chosen because the projection of light distribution resembles that of a normal distribution curve. The normal distribution curves were determined for each axial distance (5, 10, and 15 cm) by which the chartboard is away from the UV light. The fitted normal distribution curve for each axial distance was presented in **Figure 4**.

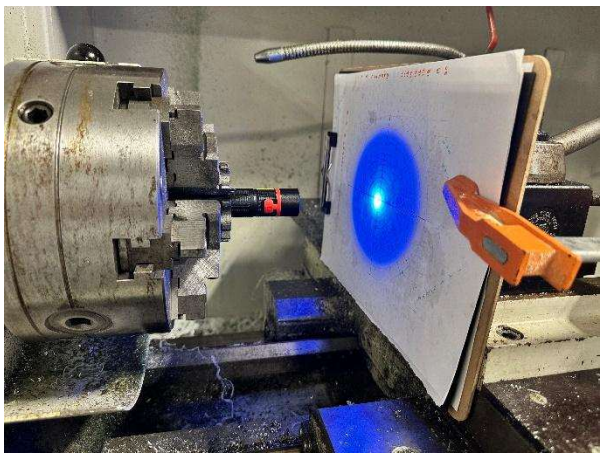


Figure 3 Experimental Setup for UV Light Characterization

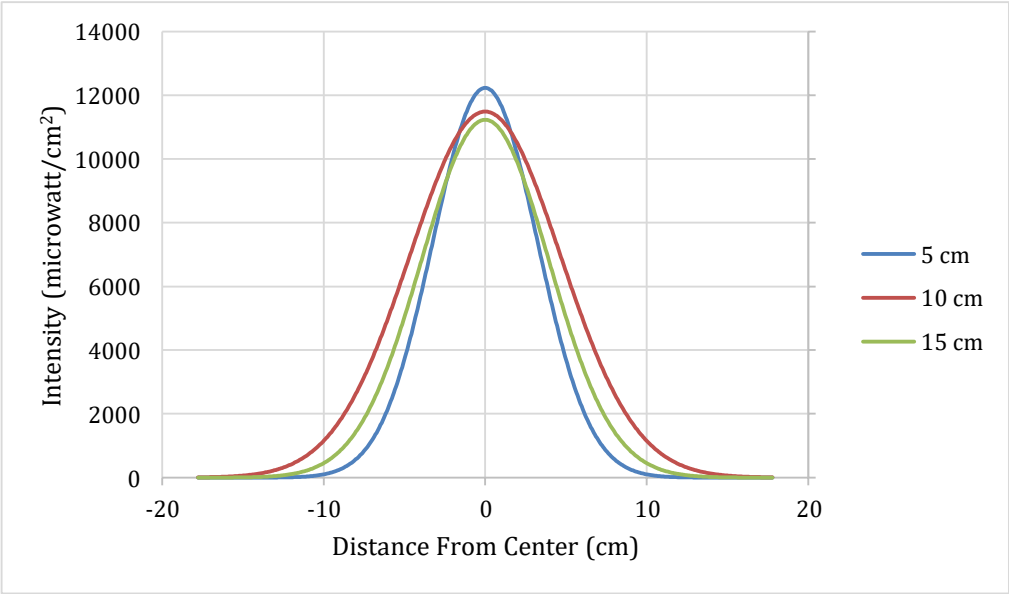


Figure 4 Fitted UV Light Intensity 2D Curves

4. Characterization of resin curing

Unlike conventional vat polymerization processes, the proposed approach relies on the curing of individually levitated droplets rather than a bulk resin reservoir. Consequently, characterization of resin curing is necessary to understand the process window and determine processing condition for experimentation. The polymer resin used in this study was commercially available photo-sensitive liquid resin developed for STL and DLP processes (commercial name *Anycubic UV tough resin*, from Shenzhen Anycubic Technology Co.,Ltd, China). The material ingredients include a photopolymer, a monomer, a photoinitiator, and additives for coloration. The photoinitiator in this resin is bis(2,4,6-trimethylbenzoyl)-phosphine oxide (BAPO), which has a wide absorption spectrum ranging from 365 to 405 nm. Successful printing out of this commercially available resin relies on the understanding of its curing properties. Although part of the chemistry contents is provided, the complete photocuring performance under UV light is not given. For the proposed droplet based Additive Manufacturing process, the required information is similar to those suitable for STL and DLP processes. Generally, photocurable polymer resin used in Additive manufacturing can be characterized by two main parameters - Critical Energy (Ec) and Penetration Depth (Dp) **[Jacobs 1992]**. Critical Energy measures the energy threshold to initiate photopolymerization, while Penetration Depth quantifies the depth where light intensity drops to 1/e of its intensity at the resin surface **[Bennett 2017]**.

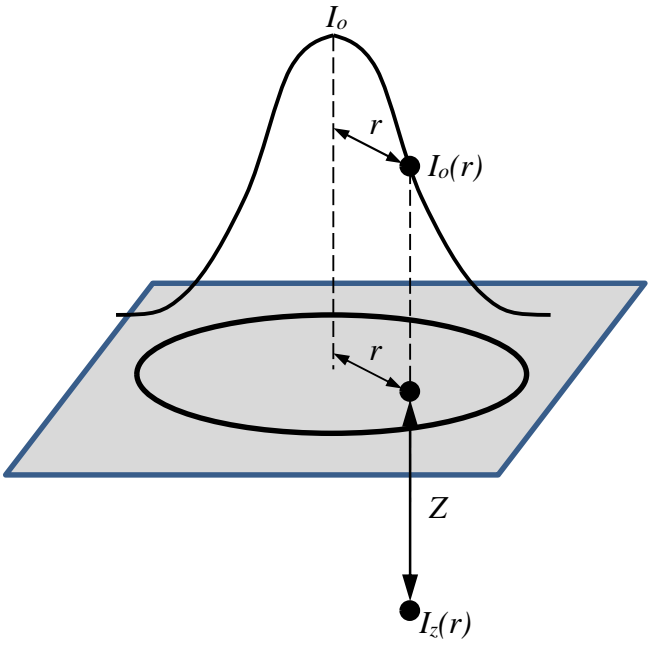


Figure 5 Gaussian Profile of Light Beam

The UV light intensity is assumed to follow Gaussian distribution as depicted in **Figure 5**, where I_o is the peak intensity corresponding to the intensity along the centerline, $I_o(r)$ denotes the intensity with a radial distance r away from the distribution centerline. Their relationship is described by **equation (1)**.

$$I_o(r) = I_o \exp\left(\frac{-2r^2}{w^2}\right) \quad (1)$$

As the light beam passes through the resin material, the intensity decreases due to the absorption and is dependent on the penetration depth. The light intensity inside the resin is modeled using Beer-Lambert law (**equation (2)**), where $I_z(r)$ represents the intensity at a depth Z.

$$I_z(r) = I_o(\mathrm{r})\exp\left(\frac{-z}{D_p}\right) \quad (2)$$

Merging **Equation (1)** and **Equation (2)**, light intensity ($I_z(r)$) at the depth Z with a radial distance r from the centerline is obtained as follows.

$$I_z(r) = I_o\exp\left(-\frac{2r^2}{w^2} - \frac{z}{D_p}\right) \quad (3)$$

The energy amount received by the resin within the exposure time duration t_o at radial distance r is then obtained as

$$E_z(r) = I_o\exp\left(-\frac{2r^2}{w^2} - \frac{z}{D_p}\right)t_o \quad (4)$$

At r=0, define the received energy amount as E_c and depth Z= Cd, **Equation (4)** is simplified as

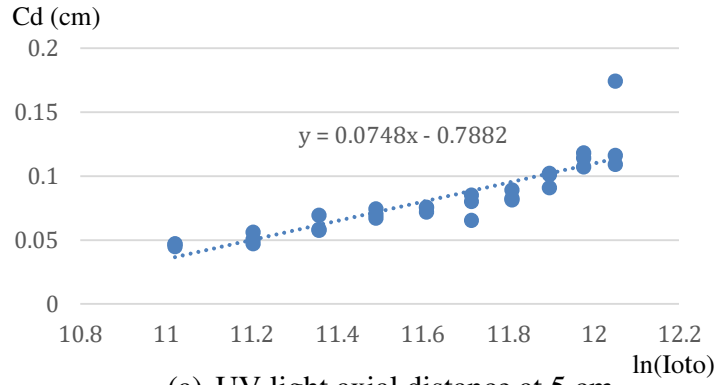
$$E_C = I_o t_o \exp\left(-\frac{C_d}{D_p}\right) \quad (5)$$

Through further rearrangement, Cd is linearly related to the term $ln(I_o\ t_o)$ as described in **Equation (6)**. This relationship renders a practical methodology to experimentally calculate the Critical Energy (Ec) and Penetration Depth (Dp) for a particular resin. Experimentally Cd can be measured given that the UV light with peak intensity I_o is exposed to the resin for time duration t_o. With a series of different exposure times applied on the fresh resin, the corresponding depth measurements of Cd allow for the plotting curves displaying the relation between Cd and $ln(I_o\ t_o)$.

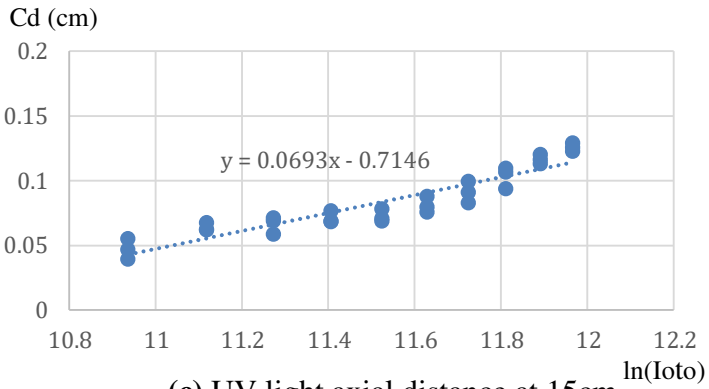
$$C_d = D_p Ln(I_o t_o) - D_p \ln E_c \quad (6)$$

In this research, the UV light with peak intensity I_o was exposed to the resin for each selected time duration t_o to create the cured resin layers. Subsequently, the cured resin layer was examined and measured on an optical comparator to obtain the corresponding depth information on Cd. Similar to the reports by **[Bennett 2017]**, the plots between Cd and $ln(I_o\ t_o)$ manifested a linear relationship with the slope equal to Dp and the intercept containing both Dp and Ec, hence allowing the calculation of Ec. **Figures 6a-c** display the relation plots between Cd and $ln(I_o\ t_o)$ with the UV light positioned at 5, 10, and 15 cm away from the resin in the experiment. For each axial distance of the UV light, exposure time duration t_o incrementally increased from 5 seconds to 14 seconds, and experiment for each exposure time duration t_o at each axial distance was repeated three times. From **Figures 6a-c,** a best fitted line was obtained, showing the linear relationship between Cd and $ln(I_o\ t_o)$ at each axial distance from the UV light, from which Dp and Ec were calculated and are presented in **Table 1**. From **Table 1**, it can be observed that neither Dp nor Ec exhibit a clear relationship with the axial distance of the

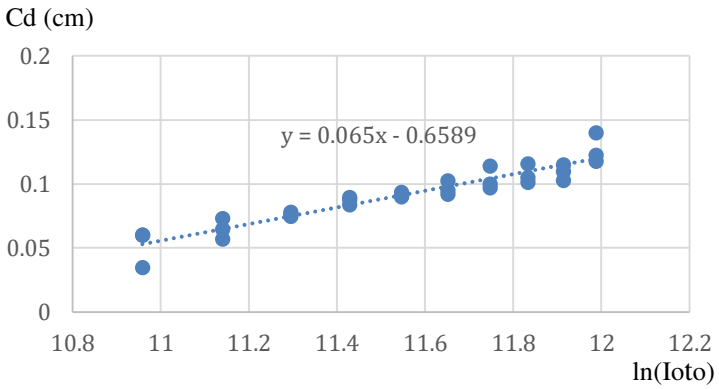
UV light from the resin surface. This finding suggests that the axial distance of UV light can be adjusted in the curing process to vary the intensity while the fundamental property of the resin's reaction to the UV light will not be altered.



(a) UV light axial distance at 5 cm



(c) UV light axial distance at 15cm



(b) UV light axial distance at 10 cm

Figure 6 Characterization of resin photopolymerization

Table 1 Calculated Dp and Ec

Distance (cm)	Dp (cm)	Ec (mJ/cm^2)
5	0.0748	37.51
10	0.0649	25.41
15	0.0693	30.25

5. Contact Angle Measurement

Contact angle measurement is a useful technique capable of evaluating the wettability of a liquid sample on a solid surface. The formation of contact angle is a result of surface tension and adhesion properties. As this additive manufacturing process used a droplet by droplet deposition approach, it is important to understand the interaction of each liquid droplet and previously solidified material. As the liquid droplet contacts the solid surface, the extent of wettability determines the profile formed between these two phases of material, influencing how the droplet spreads and attaches. In this study, droplets are deposited and cured sequentially

to form an additively manufactured structure. Therefore, contact angle measurement not only assesses the adhesion and spread of the resin droplet, but also offers insights into the surface uniformity of the printed structure surface, which is an important quality characteristic in droplet based additive manufacturing.

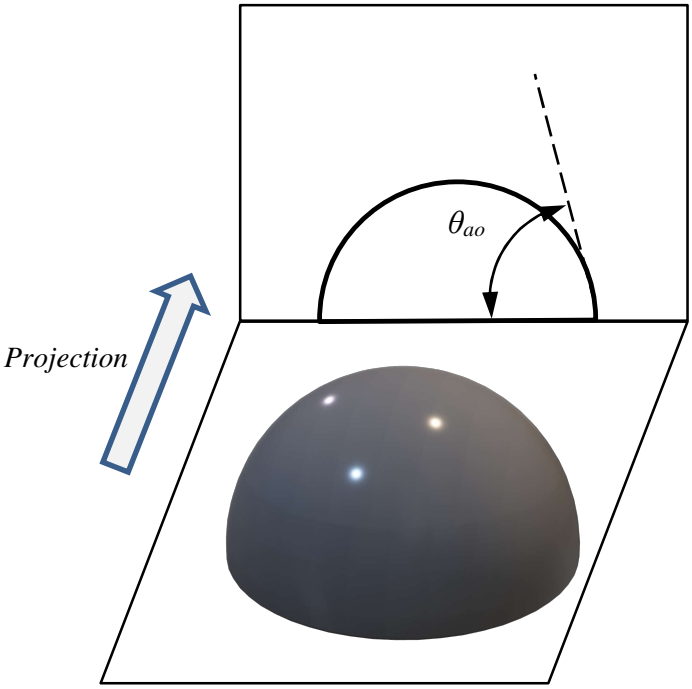


Figure 7 Measurement of intrinsic advancing contact angle

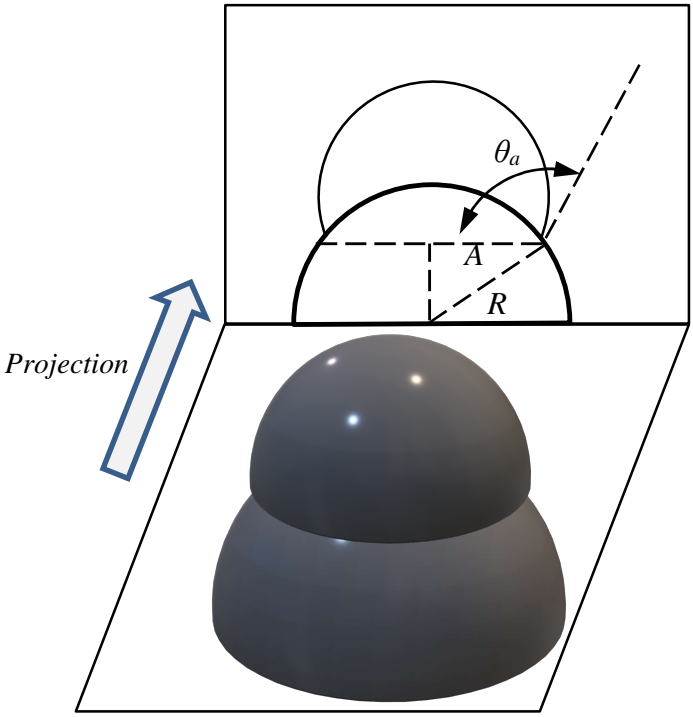


Figure 8 Measurement of apparent advancing contact angle

In this research, the contact angle was measured using the method described by **Extrand and Moon [Extrand and Moon 2008]**, as illustrated in **Figure 7 and Figure 8.** The figures have been recreated based on their work, maintaining the same symbols and terms for consistency and clarity. According to **Extrand and Moon's** observation, the profile of a droplet displays an intrinsic advancing contact angle when being placed on a flat surface; when the droplet meets with an edge on the surface, an apparent advancing contact angle forms at its profile showing the droplet being constrained. The relation between the intrinsic advancing contact angle and the apparent advancing contact angle **(Equation 7)** provides a way of calculating the quality characteristic of the additive manufacturing process.

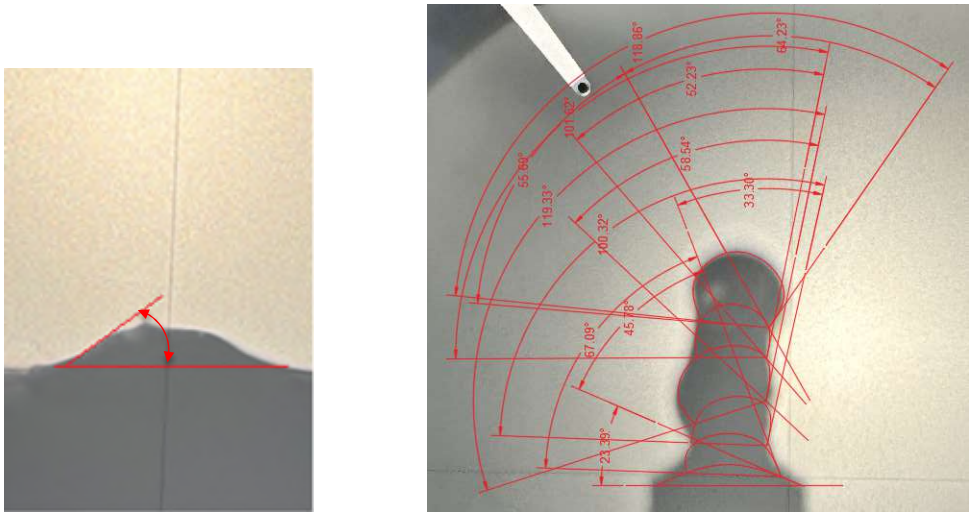
$$\theta_{ao} = \theta_a - sin^{-1}\left(\frac{A}{R}\right) \quad (7)$$ **[Extrand and Moon 2008]**

In order to measure the intrinsic advancing contact angle, a flat surface made of the same material was prepared by casting the photosensitive resin in a mold followed by a full extent curing process. Initially a droplet of liquid resin was deposited on the obtained flat surface, with their profiles projected using an optical comparator (**Figure 7**). Tangential line was drawn at the intersection of the projected image, allowing the measurement of the intrinsic advancing contact angle. The initial deposited droplet was solidified by photocuring process and prepared a curved

substrate surface for the deposition of the next droplet. In the similar way, each deposited and cured droplet forms the curve surface for the deposition of the subsequent droplet. The deposited geometry profile projected on the optical comparator allows for the measurement of the apparent advancing contact angles of each deposited droplet (**Figure 8**). Based on the experimental finding of **Extrand and Moon [Extrand and Moon 2008]**, the intrinsic advancing contact angle is not influenced by droplet volume and substrate curvature radius. Hence, the chord to radius ratio (A/R ratio, illustrated in **Figure 8**) is determined based on the measured intrinsic advancing contact angle on the flat surface and the measured apparent advancing contact angle using **Equation 8**. The A/R ratio provides an experimental approach to evaluate the surface uniformity produced by the droplet based additive manufacturing.

$$\frac{A}{R} = \sin(\theta_a - \theta_{a0}) \qquad (8)\ \textbf{[Extrand and Moon 2008]}$$

In this work, contact angle measurements were experimentally performed using an optical comparator. The profile of each cured resin droplet was projected and captured as a digital image. The acquired image was subsequently imported into AutoCAD for geometric analysis. Tangent lines were constructed at the droplet-substrate interface, and the contact angle was determined from the angle between the tangent line and the substrate surface. **Figures 9 (a) and (b)** presents representative digital images of contact angle measurements for the first droplet deposited on the substrate and for five continuous droplets, respectively. The measured contact angles not only characterize droplet spreading behavior, but also directly influence surface uniformity indicator - A/R ratio of deposited droplets through **Equation (8)**.



(a) **(b)**

Figure 9 Contact angle measurements obtained from optical comparator images: (a) single deposited droplet and (b) five consecutive deposited droplets used for A/R ratio evaluation.

6. DOE-based Process Optimization

Staircase effect is inherent to almost all additive manufacturing, leading to surface waviness. Many researchers have proposed ways of mitigating staircase effect to improve 3D printed surface quality **[Tang et al. 2024, Zhao and Guo 2020, Mathew et. al. 2023]**. Specifically, for the droplet-based additive manufacturing, A/R ratio is desired to be larger the better in order to produce a uniform surface. In our analysis of A/R ratio, we used the average A/R ratio of five continuously deposited droplets as the optimization response. **Figure 9(b)** shows an example of measuring five continuous droplets for obtaining the average A/R ratio over the structure surface.

In this research, Taguchi experiment was employed to achieve an optimal A/R ratio for continuous droplet deposition. Taguchi method is able to both effectively and efficiently optimize manufacturing processes by using orthogonal experiment design. Compared to full factor experiment design, the orthogonal experiment layout significantly reduces the number of trials, making process optimization both time and cost effective. This merit earned Taguchi method applicability in a wide range of manufacturing processes, including but not limited to machining **[Lin et.al. 2009,Fratila and Caizar 2011]**, metal forming **[Li et.al. 2006, Yan et.al. 2022]**, injection molding **[Chen et.al. 2016, Tian et.al. 2017]**, casting **[Wu and Chang 2004**, **Yang et.al. 2023,]** and 3D printing **[Jiang et.a.l. 2022, Sultana et.al. 2024]**, etc.

Taguchi experiment design accommodates both controllable factors and noise factors with the noise factors designated as the uncontrollable parameters which often exist in manufacturing research. In this research we consider four controllable factors for optimization, each in three levels and one noise factor in two levels. The first controllable factor is UV light axial distance from the resin. As discussed in **Section 4,** the light intensity follows Gaussian distribution that directly affects the resin curing. As the axial distance from the UV light to the resin changes, energy dose delivered to the resin will be different. Not only does the resin require a critical energy level to initiate the photopolymerization, but UV light intensity received by the resin also plays an influential role in controlling the extent of resin curing. By varying the UV light axial distance, the curing depth and profile can be adjusted to optimize the curing performance in the workpiece. The second parameter is time duration of curing. We chose this parameter because it determines the time extent to which the resin is exposed to the UV light. Photopolymerization is a time-sensitive process. Insufficient UV light exposure time may lead to incomplete curing of resin, resulting in improperly formed profile geometry. Undercured resin also leads to problems such as poor droplet bonding and mechanical property deterioration, both of which compromise the 3D printed structure integrity. The third parameter incorporated in the Taguchi experiment is angle of the robotic arm end effector. This angle directly affects the orientation of attachment when the droplet is being cured on the levitator. When the droplet touches the substrate during curing, it is subject to the influences from both surface tension of resin and gravity. The inclusion of robotic arm end effector angle intends to reveal their significance in the practical printing. The fourth parameter is the radial distance of the droplet location from the UV light central axis. As the UV light intensity follows a Gaussian distribution, the distance between the droplet and UV light central axis will affect the energy received by the resin droplet. The longer the radial

distance incurs the less amount of light energy for curing the droplet. We chose the radial distance as a factor in order to study its interaction with the axial distance of the UV light. The noise factor in the Taguchi experiment design is the environment light interference. Although the resin droplet is primarily cured by the UV light beam, environmental light may affect the curing process by introducing additional light exposure. This unintended light can cause additional chemical dynamics in the photopolymerization process. By introducing this noise factor, we intend to assess the robustness of the process in the environment with ambient light conditions.

Considering the four controllable factors and one noise factor, an L-9 table was adopted for the Taguchi experiment design. The L-9 table can accommodate three levels for each controllable factor, allowing the assessment of their contribution and the optimization of different parameters. **Table 2** summarizes the parameter levels for these four main controllable factors and the non-controllable factor. For UV light axial distance, the three levels were chosen at 5cm, 10cm and 15cm away from the resin. These three levels were consistent with the distances used in **Section 3** for UV light profile characterization. For time duration of curing, the selected three levels were 5 seconds, 10 seconds and 15 seconds, respectively. A Xplora plus Raman microscope (Horiba Scientific, Japan) was used to characterize the curing process. **Figure 10** shows the Raman spectra of curing results after 1, 2, 3, 4, 5, 10 and 15 seconds. The spectral peaks at approximately 1600 cm^{-1} and 2800-3100 cm^{-1} progressively changed with increasing exposure time and became stabilized when the curing time reached 10-15 seconds of curing time. The decrease of peak at 1600 cm^{-1} corresponds to the consumption of C=C double bonds in the acrylate groups, forming more single bonds, while the increase of peak at 2800-3100 cm^{-1} relates to the formation of more C-H bonds after the C=C bonds are broken as the photopolymerization progresses. These observations suggest that significant curing occurs between 5 and 15 seconds. Therefore, for the time duration of curing, the selected three levels were 5 seconds, 10 seconds and 15 seconds, representing an early, intermediate and near-complete curing stage, respectively.

Table 2: Taguchi design parameters and levels

			Levels		
Designation	**Variable**	**Unit**	1	2	3
Controllable Factors					
A	UV axial distance	cm	5	10	15
B	Time duration	Second	5	10	15
C	Angle of Robot arm	degree	180	135	225
D	Radial Distance	cm	0	0.5	1.0
Non- Controllable Factors					
1	Environmental light on				
2	Environmental light off				

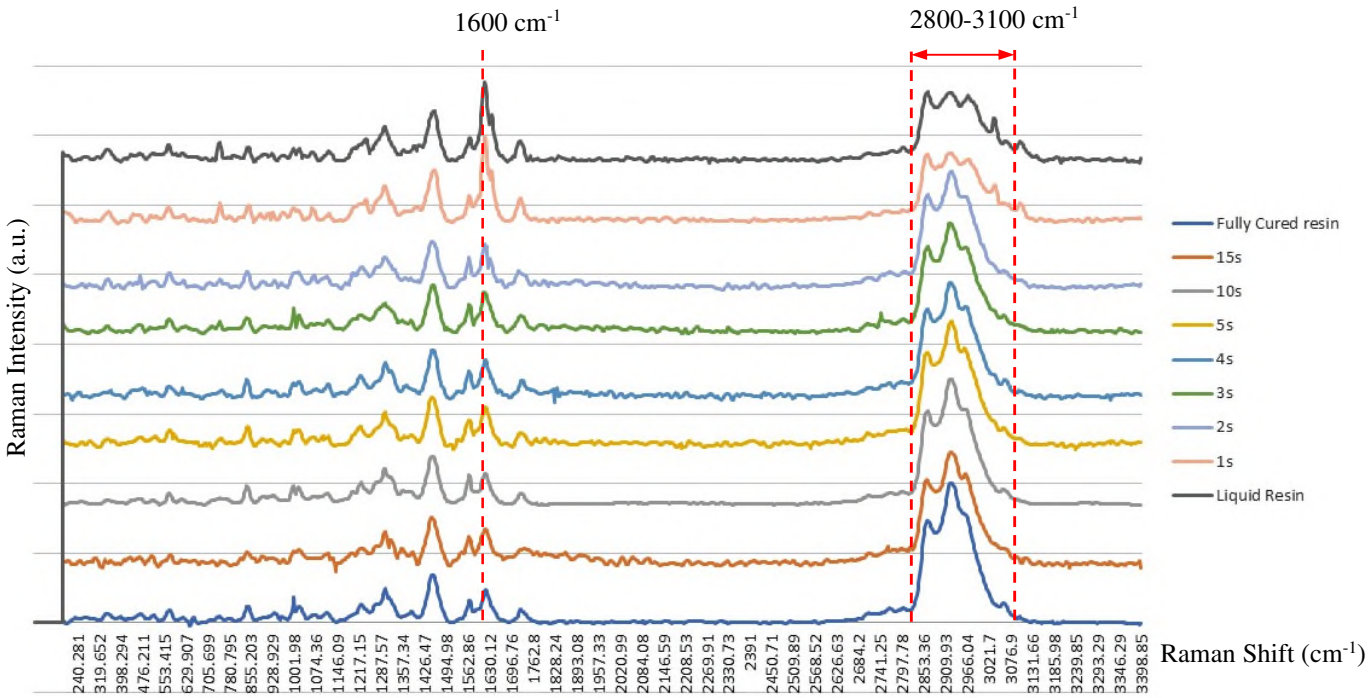


Figure 10 Raman spectra progression with increasing exposure time (Spectra vertically offset for clarity)

Table 3: Taguchi experimental results

N	Controllable Factor Levels				Non-controllable Factor		Y-Bar	S/N Ratio
	A(UV)	B(Time)	C(arm)	D(radial dist)	Ambient light off	Ambient light on		
1	1	1	1	1	0.5320	0.7256	0.6288	-4.3398
2	1	2	2	2	0.2616	0.7476	0.5046	-9.1386
3	1	3	3	3	0.5254	0.6196	0.5725	-4.9328
4	2	1	2	3	0.6186	0.5476	0.5831	-4.7335
5	2	2	3	1	0.4848	0.4934	0.4891	-6.2131
6	2	3	1	2	0.6812	0.7498	0.7155	-2.9378
7	3	1	3	2	0.5834	0.5386	0.5610	-5.0415
8	3	2	1	3	0.4688	0.5214	0.4951	-6.1429
9	3	3	2	1	0.5980	0.8048	0.7014	-3.3649

For the angle of the robotic arm end effector, the three levels were set at 180 (horizontal level), 135 (downward tilting orientation) and 225 (upward tilting orientation), as displayed in **Figure 11**. These three representative angles revealed the impact of end effector orientation on droplet deposition performance. The three radial distance levels (0, 0.5 and 1cm) were chosen to study the effect of radial distance on the curing profile. Due to the Gaussian distribution, the radial distance determines the light intensity the resin receives as its location transitions from the peak intensity at the axis (0 cm) to the reduced intensity at the light beam periphery (1cm).

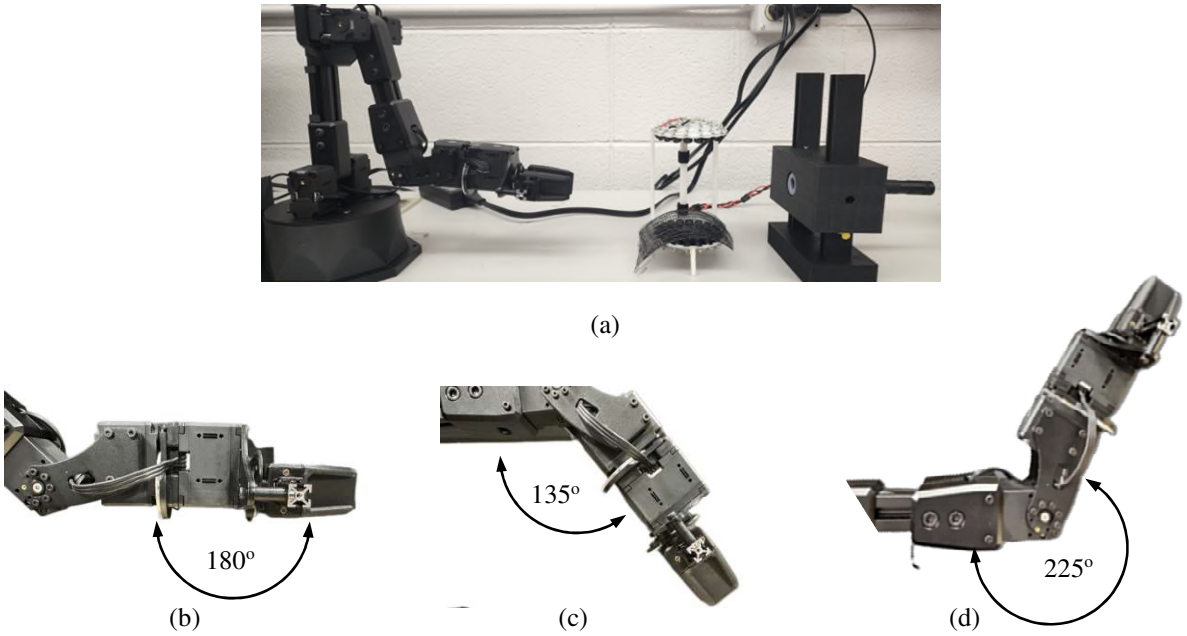


Figure 11 Robotic arm at various angles. (a) additive manufacturing setup, (b) robotic arm at 180 degrees, (c) robotic arm at 135 degrees & (d) robotic arm at 225 degrees

With the parameters and levels described above, the Taguchi L9 orthogonal array experimental result was displayed in **Table 3**. The data collected with ambient light and without ambient light for each controllable parameter combination was averaged into Y-bar values. Since the output - A/R ratio is desired to be larger the better, Signal-to-Noise (S/N) ratio was calculated using **Equation (9)**. The obtained values of Y-bar and S/N ratio allow for the determination of optimal process parameters which will yield a maximum A/R ratio on the printed structures. Each parameter must be individually analyzed to determine which level corresponds to the best performance. To this end, the graphs of A/R ratio associated with process parameters levels and the corresponding S/N ratio were made based on the summarized optimization results in **Table 3**. From **Figure 12**, the optimal parameter combination for average A/R ratio is A2B3C1D1- level two for UV axial distance (A) at 10cm, level three for time duration (B) at 15 seconds, level one for robotic arm orientation (C) at 180 degree angle and level one for radial distance (D) at 0 cm. A similar result (A2B3C1D1) is also observed when considering the S/N ratio alone as the highest S/N ratio is sought for each process parameter. The optimal parameter combination converged to the same result for both average A/R ratio and S/N ratio.

$$\eta = -10\log[(\Sigma(1/y_i^2))/n] \quad (9)$$

η: signal-to- noise ratio
y_i: individual measurements
n: number of measurements

With the optimal combination of parameter levels, it is also necessary to calculate its predicted response using **Equation (10)**. The predicted average A/R ratio for the combination A2B3C1D1 was 0.728

$$Y_{predicted} = \bar{Y}_{A*} + \bar{Y}_{B*} + \bar{Y}_{C*} + \bar{Y}_{D*} - 3\bar{Y} \quad (10)$$

Where $\bar{Y}_{A*}$, $\bar{Y}_{B*}$, $\bar{Y}_{C*}$, and $\bar{Y}_{D*}$ are mean response at the optimal level of each factor, and $\bar{Y}$ is the overall average response.

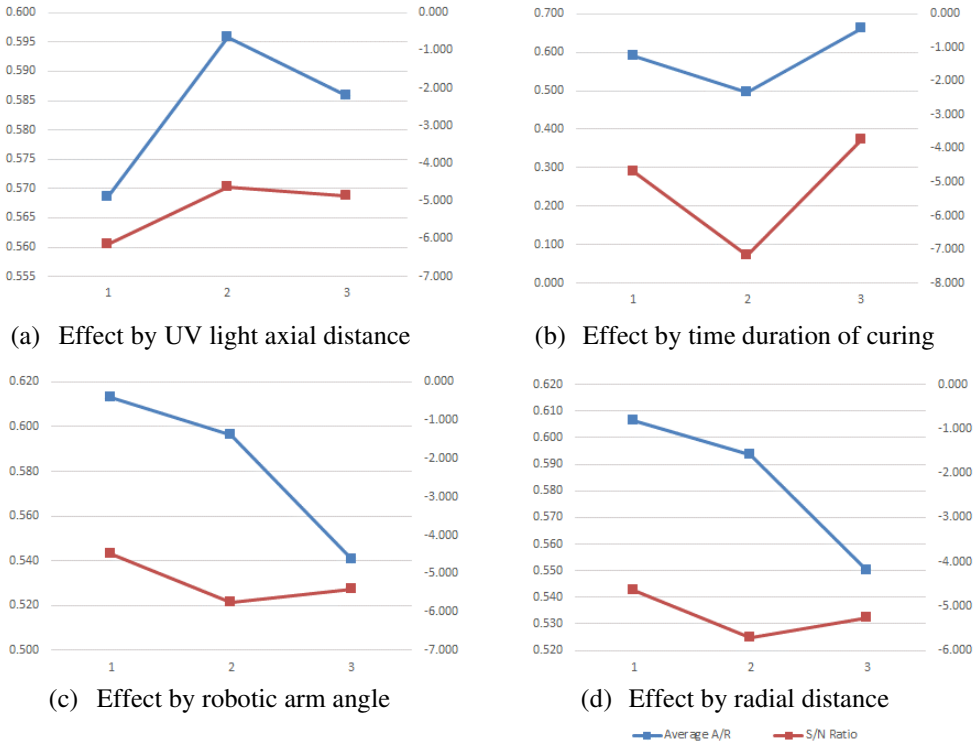


Figure 12 Response graph for Taguchi experiment

An analysis of variance (ANOVA) was conducted based on the Taguchi signal-to-noise ratios using the larger-the-better criterion. The relative influence of each controllable factor on the process performance was calculated and compared as displayed in **Figure 13**. Exposure time contributes 69.2%, ranking as the highest impacting factor followed by UV light axial distance at 14.8%, robotic arm angle at 9.6% and radial distance at 6.4%.

A T-test was performed to examine the influence of the noise factor- environmental light on the printing A/R ratio. The T-test hypothesis was formulated as

Ho: $u_{light\ on} = u_{light\ off}$

H1: $u_{light\ on} \neq u_{light\ off}$

The calculated T-value of 2.77 in this research did not exceed the critical value at alpha=1% and 16 degrees of freedom, which is equal to 2.92. From this relationship, the T-test concluded

that the null hypothesis *Ho* cannot be rejected on a 99% confidence level. Therefore our conclusion is that the environmental light does not significantly affect the printing *A/R* ratio.

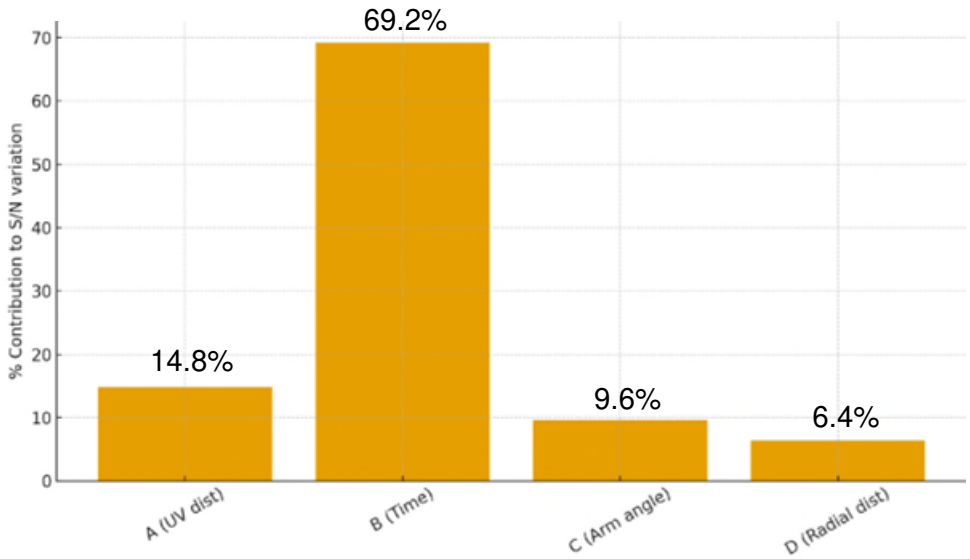


Figure 13 Controllable factor contribution to S/N ratio

A confirmation run consisting of 10 workpieces (shown in **Figure 14**) was performed as well to validate the process optimization from the Taguchi experiment. The confirmation run was implemented at the obtained optimal level combination of A2B3C1D1 with the expectation of producing comparable results to the predicted A/R ratio of 0.728. **Table 4** listed the results from the confirmation run. The ten workpieces produced an average of A/R ratio of 0.730 with a standard deviation at 0.041. The result suggests that the confirmation run output closely aligns with the predicted value of A/R ratio. The small standard deviation indicates the consistency and stability of process optimization.

Table 4 Confirmation run results

sample	1	2	3	4	5	6	7	8	9	10
Average A/R	0.675	0.770	0.746	0.729	0.680	0.756	0.717	0.682	0.746	0.796

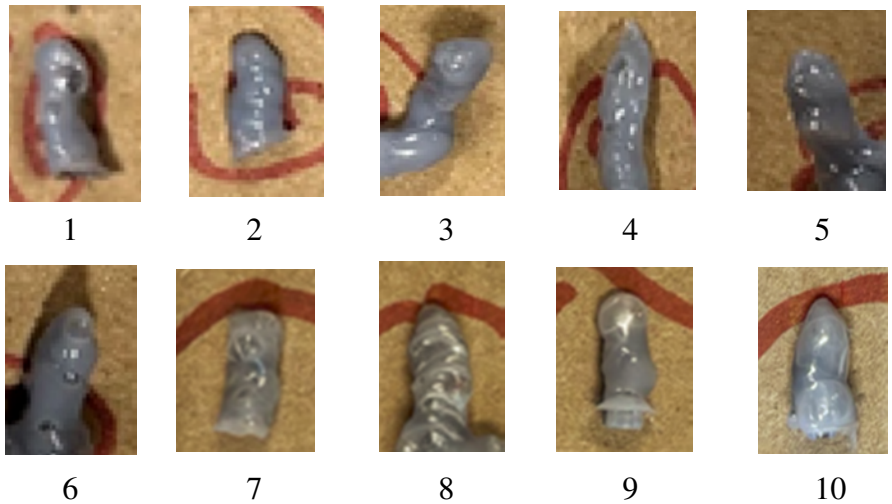


Figure 14 Confirmation run workpieces (samples 1-10) arranged in a 2×5 grid. Workpiece dimensions are approximately 0.7-1 cm. Workpieces were fabricated using optimal Taguchi parameters - A2B3C1D1

7. Discussion

This study characterized and optimized the droplet-based additive manufacturing on an acoustic levitator and robotic arm platform. By incorporating the flexibility of robotic arms, the process is different from traditional digital light processing (DLP) and stereolithography (STL) which rely on a fixed building direction and a resin tank. Specifically, we have characterized the curing property of the photocurable resin and the UV light used to accomplish the photopolymerization. The Taguchi experiment allows for the optimization of the process with selected process parameters and levels. With the identified optimal parameter levels, the predicted A/R ratio closely matched the confirmation run result. The environmental light interference was also proved statistically insignificant to the process output.

Although in Jacob's working curve the critical energy *Ec* was assumed to be a material property constant **[Jacobs 1992]**, our experimental data suggests that the value of *Ec* is influenced by the distance of the UV light from the resin surface. From **Table 1**, both *Dp* and *Ec* varied with the UV light distance; they decreased from 5cm to 10cm and then increased from 10cm to 15cm. This trend indicates that practical photopolymerization involves additional factors affecting energy penetration into the resin. At 5cm, the closer distance from the UV light resulted in a higher intensity of light energy compared to 10cm, thereby allowing more energy to penetrate into the resin. The light intensity drop explains why both *Dp* and *Ec* decreased from 5cm to 10cm. However, the resin does not cure uniformly. As the resin's top layer cures before the resin below, the cured top layer can attenuate the light intensity, reducing the light energy reaching deeper resin. At 15cm, the relatively lower light intensity caused a less aggressive curing at the top layer; therefore the blocking effect was reduced allowing better penetration to the deeper resin. This could explain why a reversed trend was observed from 10cm to 15cm.

The Taguchi experiment produced optimal results- A2B3C1D1: level two for UV axial distance (A) at 10cm, level three for time duration (B) at 15 seconds, level one for robotic arm orientation (C) at 180 degree angle and level one for radial distance (D) at 0 cm. The 10cm of UV light distance provided a balance between light intensity and curing depth. At 10cm, light intensity is moderate, resulting in less excessive curing at the top layer and providing better penetration of light energy to deeper resin. This will impart the curing process with better predictability as shown in **Figure 6**, where the working curve at 10cm (**Figure 6(b)**) displayed best linearity among the three UV axial distances. The curing time of 15 seconds indicates that a longer curing time will ensure enough light energy delivered to deeper resin, contributing to a solid 3D printed profile. Increasing curing time will also offset the attenuation of light energy due to the formation of the cured top layer. The selection of 10cm distance and 15 seconds curing time together suggest that a relative medium UV light distance coupled with longer curing time allow for better light energy absorption at deeper resin with a predictable curing depth. As the UV light intensity follows a Gaussian distribution and was placed central to the droplet, both the robotic arm orientation angle (at 180 degree) and the radial distance (at 0 cm) were selected to make

the droplet receive even light intensity variation. Deviation from the selected levels for these two factors could result in uneven exposure to the light source, leading to asymmetrical curing and hence a poor A/R ratio as the output.

However, the current experiment also comes along with limitations that should be acknowledged for future exploration. The contact angle measurement in this research was based on 2D profile projections which may miss important 3D features on the actual cured droplet surface. In our future work, an average A/R ratio and its standard deviation along the printing direction obtained from 3D profile measurement can be used as the output quality characteristics. Additionally, the research did not take into account fluid dynamics of resin during the curing process. The interaction between droplets and substrates depends on the surface tension and viscosity which are both varying due to the phase change and heat generation from UV light curing. Further, our Taguchi experimental design tested limited parameter levels for each factor. Although requiring less number of trials for process optimization, it may miss the complex nonlinear relationship among process parameters. Thus, including additional levels and repeating experiments with fine-tuned levels would reveal more insight of the process behavior.

8 Conclusion

This paper describes the concept, implementation and experimental optimization of a robotic arm assisted droplet based additive manufacturing system. The system integrated a robotic arm for maneuvering, an acoustic levitator for droplet suspension, and a UV light for photocuring the droplet. By incorporating acoustic levitation and robotic manipulation, the droplet based additive manufacturing setup eliminates the need of a single build direction, the usage of a resin tank and support structures. Moreover, it enables the non-planar material deposition. Therefore, the system offers an approach of contactless manufacturing and simplifies the post-processing of printed workpieces.

Key steps of implementing the additive manufacturing system were detailed, including the UV light profile characterization, resin property characterization, contact angle measurement. A Taguchi experiment based process optimization determined the optimal combination of process parameters. While this paper focused on the characterization and process optimization of one commercial resin, the methodology can be extended to other photocurable resins.

Future research efforts will be directed towards the following areas. (1) developing a comprehensive model for the process using governing Physics laws; (2) integrating real-time feedback systems for process monitoring and on-line quality control; (3) exploring broader printing material capabilities and expanding the current system to a multi-material additive manufacturing platform.

References

[1] Li Y, Zhang J. Multi-criteria GA-based Pareto optimization of building direction for rapid prototyping. The International Journal of Advanced Manufacturing Technology. 2013 Nov;69:1819-31.

[2] Rattanawong W, Masood SH, Iovenitti P (2001) A volumetric approach to part-build orientations in rapid prototyping. J Mater Process Technol 119(1–3):348–353

[3] Masood SH, Rattanawong W (2002) A generic part orientation system based on volumetric error in rapid prototyping. Int J Adv Manuf Technol 19(3):209–216

[4] Kumar C, Choudhury AR (2005) Volume deviation in direct slicing. Rapid Prototyping J 11(3):174–184

[5] Shen H, Guo S, Fu J, Lin Z. Building orientation determination based on multi-objective optimization for additive manufacturing. 3D Printing and Additive Manufacturing. 2020 Aug 1;7(4):186-97.

[6] Selvam A, Mayilswamy S, Whenish R, Naresh K, Shanmugam V, Das O. Multi-objective optimization and prediction of surface roughness and printing time in FFF printed ABS polymer. Scientific Reports. 2022 Oct 7;12(1):16887.

[7] Günaydın AC, Yıldız AR, Kaya N. Multi-objective optimization of build orientation considering support structure volume and build time in laser powder bed fusion. Materials Testing. 2022 Mar 28;64(3):323-38.

[8] Matos, M.A., Rocha, A.M.A.C. & Costa, L.A. Many-objective optimization of build part orientation in additive manufacturing. Int J Adv Manuf Technol 112, 747–762 (2021).

[9] Jee H, Kim M. Spherically curved layer (SCL) model for metal 3-D printing of overhangs. Journal of Mechanical Science and Technology. 2017 Dec;31:5729-35.

[10] Duarte J, Espírito Santo I, T. Monteiro MT, F. Vaz AI. Curved layer path planning on a 5-axis 3D printer. Rapid Prototyping Journal. 2022 Mar 29;28(4):629-36.

[11] Hong F, Lampret B, Myant C, Hodges S, Boyle D. 5-axis multi-material 3D printing of curved electrical traces. Additive Manufacturing. 2023 May 25;70:103546.

[12] Xie F, Chen L, Li Z, Tang K. Path smoothing and feed rate planning for robotic curved layer additive manufacturing. Robotics and Computer-Integrated Manufacturing. 2020 Oct 1;65:101967.

[13] Fry NR, Richardson RC, Boyle JH. Robotic additive manufacturing system for dynamic build orientations. Rapid prototyping journal. 2020 May 14;26(4):659-67.

[14] Fang G, Zhang T, Huang Y, Zhang Z, Masania K, Wang CC. Exceptional mechanical performance by spatial printing with continuous fiber: Curved slicing, toolpath generation and physical verification. Additive Manufacturing. 2024 Feb 25;82:104048.

[15] İpekçi A, Ekici B. An innovative composite elbow manufacturing method with 6-axis robotic additive manufacturing for fabrication of complex composite structures. Journal of Thermoplastic Composite Materials. 2024 Jan;37(1):402-25.

[16] Long C, Jiang L, Xiong S, Liu Z, Liu C, Chen Z. Effective post-cleaning strategy for vat photopolymerization 3D printed complex-structured polymer-derived ceramics. Additive Manufacturing. 2024 Aug 25;94:104456.

[17] Katheng A, Prawatvatchara W, Tonprasong W, Namano S, Kongkon P. Effect of Postrinsing Times and Methods on Surface Roughness, Hardness, and Polymerization of 3D-Printed Photopolymer Resin. European Journal of Dentistry. 2025 Feb;19(01):154-64.

[18] Mayer, J., Stawarczyk, B., Vogt, K. et al. Influence of cleaning methods after 3D printing on two-body wear and fracture load of resin-based temporary crown and bridge material. Clin Oral Invest 25, 5987–5996 (2021).

[19] Lambart AL, Xepapadeas AB, Koos B, Li P, Spintzyk S. Rinsing postprocessing procedure of a 3D-printed orthodontic appliance material: Impact of alternative post-rinsing solutions on the roughness, flexural strength and cytotoxicity. Dental Materials. 2022 Aug 1;38(8):1344-53.

[20] Jin G, Gu H, Jang M, Bayarsaikhan E, Lim JH, Shim JS, Lee KW, Kim JE. Influence of postwashing process on the elution of residual monomers, degree of conversion, and mechanical properties of a 3D printed crown and bridge materials. Dental Materials. 2022 Nov 1;38(11):1812-25.

[21] Xu Y, Xepapadeas AB, Koos B, Geis-Gerstorfer J, Li P, Spintzyk S. Effect of post-rinsing time on the mechanical strength and cytotoxicity of a 3D printed orthodontic splint material. Dental Materials. 2021 May 1;37(5):e314-27.

[22] Hwangbo NK, Nam NE, Choi JH, Kim JE. Effects of the washing time and washing solution on the biocompatibility and mechanical properties of 3D printed dental resin materials. Polymers. 2021 Dec 16;13(24):4410.

[23] Oh R, Lim JH, Lee CG, Lee KW, Kim SY, Kim JE. Effects of washing solution temperature on the biocompatibility and mechanical properties of 3D-Printed dental resin material. Journal of the Mechanical Behavior of Biomedical Materials. 2023 Jul 1;143:105906.

[24] Ye F, Qiu Z, Dai H, Zhou X, Xu D, Yan L, Dai N. Acoustic manipulation for metal additive manufacturing powder sorting. Ultrasonics. 2026 Dec 14:107926.

[25] Chen H, Bansal S, Plasencia DM, Di-Silvio L, Huang J, Subramanian S, Hirayama R. Omnidirectional and Multi-Material In Situ 3D Printing Using Acoustic Levitation. Advanced Materials Technologies. 2025 May;10(9):2401792.

[26] Foresti D, Kroll KT, Amissah R, Sillani F, Homan KA, Poulikakos D, Lewis JA. Acoustophoretic printing. Science advances. 2018 Aug 31;4(8):eaat1659.

[27] P.F. Jacobs, Fundamentals of stereo lithography, Proceedings of Solid Free Form Symposium (1992)
196-211.

[28] Bennett J. Measuring UV curing parameters of commercial photopolymers used in additive manufacturing, Addit. Manuf. 18 (2017) 203–212.

[29] Extrand CW, Moon SI. Contact angles on spherical surfaces. Langmuir. 2008 Sep 2;24(17):9470-3.

[30] Tang P, Zhao X, Shi H, Hu B, Ding J, Yang B, Xu W. A review of multi-axis additive manufacturing: potential, opportunity and challenge. Additive Manufacturing. 2024 Mar 11:104075.

[31] Zhao D, Guo W. Shape and performance controlled advanced design for additive manufacturing: a review of slicing and path planning. Journal of Manufacturing Science and Engineering. 2020 Jan 1;142(1):010801.

[32] Mathew A, Kishore SR, Tomy AT, Sugavaneswaran M, Scholz SG, Elkaseer A, Wilson VH, John Rajan A. Vapour polishing of fused deposition modelling (FDM) parts: a critical review of different techniques, and subsequent surface finish and mechanical properties of the post-processed 3D-printed parts. Progress in Additive Manufacturing. 2023 Dec;8(6):1161-78.

[33] Lin YC, Wang AC, Wang DA, Chen CC. Machining performance and optimizing machining parameters of Al2O3–TiC ceramics using EDM based on the Taguchi method. Materials and manufacturing processes. 2009 Apr 6;24(6):667-74.

[34] Fratila D, Caizar C. Application of Taguchi method to selection of optimal lubrication and cutting conditions in face milling of AlMg3. Journal of Cleaner Production. 2011 Apr 1;19(6-7):640-5.

[35] Li B, Nye TJ, Metzger DR. Multi-objective optimization of forming parameters for tube hydroforming process based on the Taguchi method. The International Journal of Advanced Manufacturing Technology. 2006 Feb;28(1):23-30.

[36] Yan P, Li F, Liu Z, Li L. Sensitivity analysis of die structural and process parameters in porthole die extrusion of magnesium alloy tube using Taguchi method. The International Journal of Advanced Manufacturing Technology. 2022 Apr;119(11):8039-56.

[37] Chen WC, Nguyen MH, Chiu WH, Chen TN, Tai PH. Optimization of the plastic injection molding process using the Taguchi method, RSM, and hybrid GA-PSO. The International Journal of Advanced Manufacturing Technology. 2016 Apr;83(9):1873-86.

[38] Tian M, Gong X, Yin L, Li H, Ming W, Zhang Z, Chen J. Multi-objective optimization of injection molding process parameters in two stages for multiple quality characteristics and energy efficiency using Taguchi method and NSGA-II. The International Journal of Advanced Manufacturing Technology. 2017 Mar;89(1):241-54.

[39] Wu DH, and Chang MS. Use of Taguchi method to develop a robust design for the magnesium alloy die casting process. Materials Science and Engineering: A. 2004 Aug 15;379(1-2):366-71.

[40] Yang WC, Yang JY, Kim RC, Om MS, Kim UH, Ri WS, Sok SH. Multi-attribute optimization and influence assessment methodology of casting process parameters combined with

integrated MADM and Taguchi method. The International Journal of Advanced Manufacturing Technology. 2023 Nov;129(1):681-95.

[41] Jiang CP, Cheng YC, Lin HW, Chang YL, Pasang T, Lee SY. Optimization of FDM 3D printing parameters for high strength PEEK using the Taguchi method and experimental validation. Rapid Prototyping Journal. 2022 Jun 29;28(7):1260-71.

[42] Sultana J, Rahman MM, Wang Y, Ahmed A, Xiaohu C. Influences of 3D printing parameters on the mechanical properties of wood PLA filament: an experimental analysis by Taguchi method. Progress in Additive Manufacturing. 2024 Aug;9(4):1239-51.

Statements and Declarations

Funding:

The authors are grateful to the financial support from the Student Engagement Award at Bradley University under the grant no. 1331466.

Competing Interests:

The authors have no relevant financial or non-financial interests to disclose.

Data availability:

Data available upon request